

# Structural investigation of the “tripled-tetragonal-tungsten-bronze” phases $\text{Sr}_2\text{M}_{10-x}\text{O}_{27-y}$ ( $\text{M} = \text{Nb}, \text{Ta}$ )

Justin B. Felder<sup>a</sup>, Winnie Wong-Ng<sup>b</sup>, Rania A. Qabbani<sup>a</sup>, Robert S. Roth<sup>b,1</sup>, Brian H. Toby<sup>c</sup>, Julia Y. Chan<sup>a,\*</sup>

<sup>a</sup> Department of Chemistry and Biochemistry, University of Texas at Dallas, 800 W. Campbell Road, Richardson, TX 75080, United States

<sup>b</sup> Materials Science and Engineering Laboratory, National Institute of Standards and Technology, Gaithersburg, MD 20899, United States

<sup>c</sup> Advanced Photon Source, Argonne National Laboratory, 9700 S. Cass Avenue, Lemont, IL 60439, United States

## ARTICLE INFO

### Article history:

Received 21 February 2019

Accepted 3 June 2019

Available online 15 June 2019

### Keywords:

Tetragonal tungsten bronze

Ceramics synthesis

X-ray and neutron diffraction

Oxides

Rietveld refinement

## ABSTRACT

$\text{Sr}_2\text{Nb}_{10}\text{O}_{27}$  and  $\text{Sr}_2\text{Ta}_{10-x}\text{O}_{27-y}$  exhibit the tripled tetragonal-tungsten-bronze (TTTB)-related superstructures. In contrast to  $\text{Sr}_2\text{Ta}_{10-x}\text{O}_{27-y}$ , where an extended solid solution was found,  $\text{Sr}_2\text{Nb}_{10}\text{O}_{27}$  only forms a narrow range of solid solution,  $\text{Sr}_{1-x}\text{Nb}_{10}\text{O}_{27-z}$  ( $0 \leq x \leq 0.04$ ). Serial X-ray and neutron diffraction studies show that both compounds can be modelled in the orthorhombic *Pba2* space group. Lattice parameters obtained from powder X-ray refinements are  $a = 12.3887(14)$  Å,  $b = 37.103(4)$  Å,  $c = 3.866(2)$  Å, for  $\text{Sr}_2\text{Ta}_{10-x}\text{O}_{27-y}$ , and  $a = 12.3888(2)$  Å,  $b = 36.9839(5)$  Å, and  $c = 3.94027(3)$  Å for  $\text{Sr}_2\text{Nb}_{10}\text{O}_{27}$ . Neutron Rietveld refinements of both structures revealed the possible reason for the differing solid solution behavior. For  $\text{Sr}_2\text{Nb}_{10}\text{O}_{27}$ , all Nb sites are fully occupied, whereas in  $\text{Sr}_2\text{Ta}_{10-x}\text{O}_{27-y}$ , three out of the nine crystallographically unique Ta sites were shown to be partially occupied. Charge adjustment is therefore possible by increasing the Sr concentration, leading to a solid solution series and smaller Ta/Sr ratio as compared to  $\text{Sr}_2\text{Nb}_{10}\text{O}_{27}$ . In the TTTB-related structures, Nb and Ta ions both occupy octahedral and pentagonal bipyramidal coordination sites. Layers of interconnected corner-shared octahedra were found parallel to the *ab* plane, with 3-, 4- and 5-fold tunnels found in the structure running parallel to the *c*-axis. Sr ions partially fill the 4- and 5-fold tunnels.

© 2019 Elsevier Ltd. All rights reserved.

## 1. Introduction

The tungsten bronze (TB) family of compounds [1–3] possess both structural flexibility and chemical versatility and is found in a great number of systems with technological applications. Tungsten bronze oxides with the triple or tetragonal tungsten-bronze (TB) structure type have been shown to have technological applications such as ferroelectricity and nonlinear optical properties due to their versatile structure that exhibit tunnel-like channels [4]. Tetragonal potassium lithium niobate and barium sodium niobate,  $\text{K}_3\text{Li}_2\text{Nb}_5\text{O}_{15}$  and  $\text{Ba}_2\text{NaNb}_5\text{O}_{15}$  have been found to be excellent nonlinear optical materials for second harmonic generation [5]. Additionally, the tetragonal tungsten bronze  $\text{KNb}_2\text{O}_5\text{F}$  can be used as a potential sodium ion battery anode due to its framework resembling tunnels that facilitate the transport of ions [6]. Recently, TBs have been of keen interest in the drive for green energy, particularly the triple TBs that have been considered as piezoelectric and pyroelectric materials [7]. To achieve maximum performance, a pyroelectric must have a high pyroelectric coefficient,

and a minimum dielectric constant. This is verified by calculating the figure of merit (*F*), which is an important heat-sensing parameter of pyroelectric materials [8].

The tungsten bronze structure consists of a framework of regular or distorted corner-sharing  $\text{MO}_6$  octahedra. With the common corners as hinges, the M–O–M angles vary to form tunnels of different sizes and shapes. The occupancy of tunnel sites and the size and charge of the guest metal ions impact the properties to a large extent. Tungsten bronzes can be categorized into three general structure types: the A-cation deficient perovskite type, the hexagonal tungsten bronze (HTB) and the tetragonal tungsten bronze (TTB). In TTB, the corner-sharing octahedra form a network which contains 3-, 4-, and 5-fold tunnels, whereas in the hexagonal tungsten bronze (HTB) structure, 6-membered tunnels are found [9,10]. Some of these tunnel sites are available for guest atoms.

The lattice parameters of the tetragonal tungsten bronze structure are  $a \approx 12.4$  Å and  $c \approx 3.9$  Å. Craig and Stephenson determined the lattice parameters of  $\text{Nb}_8\text{W}_9\text{O}_{47}$  to be based on a 9-fold TTB subcell unit [11]. Jamieson et al. determined the lattice parameters of  $(\text{Ba}_{0.27}\text{Sr}_{0.76})\text{Nb}_2\text{O}_{5.78}$  to be a 3-fold expansion of the TTB prototype along both *a* and *b*-axes [12]. During the study of the phase equilibria of the  $\text{Nb}_2\text{O}_5$ – $\text{WO}_3$  system, Roth and Waring found a variety of compounds that crystallized with triple tetragonal-tungsten

\* Corresponding author.

E-mail address: [Julia.Chan@utdallas.edu](mailto:Julia.Chan@utdallas.edu) (J.Y. Chan).

<sup>1</sup> Deceased July 16, 2012.

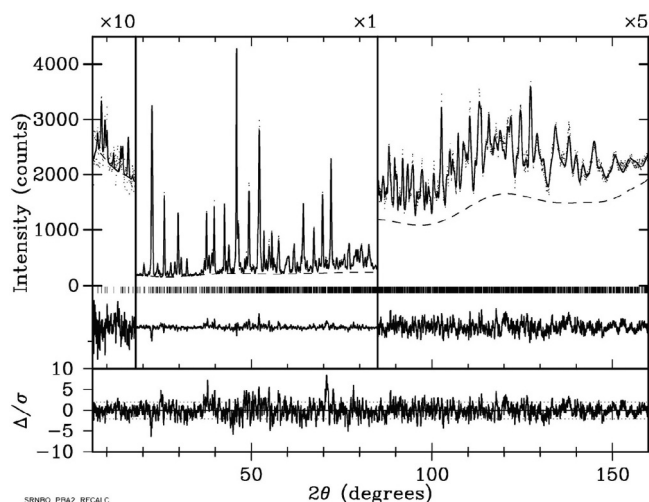


Fig. 1. Neutron Rietveld refinement results for  $\text{Sr}_2\text{Nb}_{10}\text{O}_{27}$ . The difference map is shown below the diffraction pattern.

bronze (TTTB) unit cells (i.e.  $\text{Nb}_8\text{W}_9\text{O}_{47}$ :  $a = 36.692 \text{ \AA}$ ,  $b = 12.191 \text{ \AA}$ , and  $c = 3.945 \text{ \AA}$ ; and  $\text{Nb}_{12}\text{W}_{11}\text{O}_{63}$ :  $a = 36.740 \text{ \AA}$ ,  $b = 12.195 \text{ \AA}$ , and  $c = 3.951 \text{ \AA}$ ) [13].

In the process of phase equilibrium studies of the  $\text{SrO-Ta}_2\text{O}_5$  (Fig. 1) [14] and  $\text{SrO-Nb}_2\text{O}_5$  systems [15], we found that although the structures of both  $\text{Sr}_2\text{Ta}_{10-x}\text{O}_{27-y}$  and  $\text{Sr}_2\text{Nb}_{10}\text{O}_{27}$  are related to the TTTB type, there are differences in the structural details. Furthermore, the structural chemistry of these two compounds is quite challenging. For example, while  $\text{Sr}_2\text{Nb}_{10}\text{O}_{27}$  was reported to have a complex superstructure (both  $a$  and  $b$  tripled) [16], single crystals of this composition grown in this laboratory from  $\text{SrO:Bi}_2\text{O}_3$  and  $\text{B}_2\text{O}_3$  fluxes show only the tripled  $b$ -axis (see Buerger precession photographs, Fig. S1). Secondly, despite rather different chemical formulas of  $\text{Sr}_2\text{Nb}_{10}\text{O}_{27}$  and  $\text{Sr}_2\text{Ta}_{10-x}\text{O}_{27-y}$ , preliminary work indicates these two phases having similar cell parameters and space group. Thirdly, while  $\text{Sr}_2\text{Nb}_{10}\text{O}_{27}$  was reported to be a nominally stoichiometric compound [15], in the  $\text{SrO-Ta}_2\text{O}_5$  system, a TTB-type solid solution was found to have a composition ranging from  $\text{SrTa}_2\text{O}_6$  to  $\text{SrTa}_4\text{O}_{11}$  [14]. The crystallographic reason for the extensive solid solution in the tantalate system, as compared to the narrow TTB-type solid solution in the niobate system, has remained unclear. Therefore, an understanding of the crystallochemical reason for the similar lattice parameters with different solid solution behavior of the TTTB compounds,  $\text{Sr}_2\text{Nb}_{10}\text{O}_{27}$  and  $\text{Sr}_2\text{Ta}_{10-x}\text{O}_{27-y}$ , is the primary goal of this investigation.

$\text{Sr}_2\text{Nb}_{10}\text{O}_{27}$  was first discovered in 1982 during investigations of the  $\text{SrO-Nb}_2\text{O}_5$  phase space [17], with more recent investigations focusing on thermal properties [18,19]. For the  $\text{Sr}_2\text{Ta}_{10-x}\text{O}_{27-y}$  phase, the only reported experimental or calculated patterns are those of the HTB-type [9,10], and of a TTB structure which has a large tetragonal cell ( $a = 52.59 \text{ \AA}$ , and  $c = 7.73 \text{ \AA}$ ) [20]. Preparation of reference X-ray diffraction patterns of TTTB-  $\text{Sr}_2\text{Ta}_{10-x}\text{O}_{27-y}$  and  $\text{Sr}_2\text{Nb}_{10}\text{O}_{27}$  is another goal of this study.

## 2. Experimental<sup>2</sup>

### 2.1. Synthesis

Polycrystalline samples of  $\text{Sr}_2\text{Ta}_{10-x}\text{O}_{27-y}$  and  $\text{Sr}_2\text{Nb}_{10}\text{O}_{27}$  were prepared by solid-state reaction of stoichiometric amounts of

$\text{SrCO}_3$  (powder, 99.999%) and  $\text{Ta}_2\text{O}_5$  (powder 99.993%) or  $\text{Nb}_2\text{O}_5$  (powder, 99.998%). Mixtures were pressed in a pelletizing die. The compacted powders were heat treated in air for 36 h each at  $750 \text{ }^\circ\text{C}$ ,  $1000 \text{ }^\circ\text{C}$ ,  $1200 \text{ }^\circ\text{C}$ , and  $1250 \text{ }^\circ\text{C}$  for  $\text{Sr}_2\text{Nb}_{10}\text{O}_{27}$  and up to  $1500 \text{ }^\circ\text{C}$  for  $\text{Sr}_2\text{Ta}_{10-x}\text{O}_{27-y}$ . Between heat treatments, samples were reground and repelletized for homogeneity. To investigate solid solution formation of  $\text{Sr}_2\text{Nb}_{10}\text{O}_{27}$  ( $\text{SrO:Nb}_2\text{O}_5 = 28.57:71.43$ ), three samples with  $\text{SrO:Nb}_2\text{O}_5$  molar ratio of (30:70), (27:73), and (25:75) were prepared, with a maximum heating temperature of  $1275 \text{ }^\circ\text{C}$ .

### 2.2. Neutron diffraction

Since neutron diffraction is a powerful technique to determine oxygen atom positions and occupancies, data for  $\text{Sr}_2\text{Nb}_{10}\text{O}_{27}$  were collected with the BT-1 diffractometer (32 detectors) at the Center for Neutron Research of the National Institute of Standards and Technology using a  $\text{Cu (311)}$  monochromator ( $\lambda = 1.5396 \text{ \AA}$ ). Detailed information of this research facility is described on the NIST Web site [21]. Samples were loaded in a 6 mm diameter vanadium container and measurements were made under ambient conditions. Rietveld refinements [22–24] were performed using the GSAS software [25,26]. The experimental parameters refined during the Rietveld process included scale factor, background function (Chebyshev polynomials), lattice parameters, and atomic coordinates. Special attention was paid to space group selection, choosing between  $Pbam$  and  $Pba2$ . Neutron Rietveld refinements using  $Pba2$  gave considerably better  $R$  values than the space group  $Pbam$ . Statistical analyses using an  $F$ -test [21] confirmed that space group  $Pba2$  provides statistically better fits for both compounds. The initial structural model was obtained by single-crystal X-ray diffraction. The  $R$  values from the neutron refinements for  $\text{Sr}_2\text{Nb}_{10}\text{O}_{27}$  are  $R_{\text{wp}} = 7.91$  and  $R_{\text{Bragg}} = 3.982$ . Fig. 1 illustrates the results of neutron Rietveld refinement for  $\text{Sr}_2\text{Nb}_{10}\text{O}_{27}$ . Table 1 provides the lattice parameters for  $\text{Sr}_2\text{Nb}_{10}\text{O}_{27}$  from neutron refinements and Table S1 provides the atomic positions from the refinement.

### 2.3. X-ray diffraction

Powder X-ray diffraction data were collected with a Bruker D8 Advance powder diffractometer operating at 40 kV and 30 mA with  $\text{Cu K}\alpha$  radiation ( $\lambda = 1.54184 \text{ \AA}$ ) with a LYNXEYE detector. Data were collected in the  $2\theta$  range of  $10\text{--}80^\circ$  with a step size of  $0.02^\circ$  with an exposure time of 0.5 s. Preliminary structural models were obtained from single-crystal X-ray diffraction. Precession images are shown in Fig. S1. Rietveld refinements were performed with the Topas software [27]. The refined lattice parameters are pro-

Table 1  
Lattice parameters (space group  $Pba2$ ).

Neutron	$\text{Sr}_2\text{Nb}_{10}\text{O}_{27}$	
$a$ (Å)	12.3903(5)	
$b$ (Å)	37.0041(14)	
$c$ (Å)	3.94505(9)	
$V$ (Å <sup>3</sup> )	1808.77(11)	
$wR_p$	5.55	
$R_p$	4.48	
$\chi^2$	2.794	
X-ray	$\text{Sr}_2\text{Nb}_{10}\text{O}_{27}$	$\text{Sr}_2\text{Ta}_8\text{O}_{22}$
$a$ (Å)	12.3888(2)	12.3887(14)
$b$ (Å)	36.9839(5)	37.103(4)
$c$ (Å)	3.94027(3)	3.866(2)
$V$ (Å <sup>3</sup> )	1805.37(4)	1777.3(3)
$R_{\text{wp}}$	10.09	19.17
$R_{\text{Bragg}}$	5.179	7.846
$R_{\text{exp}}$	2.89	2.81
Goodness-of-fit (GOF)	3.50	6.83

<sup>2</sup> The purpose of identifying the equipment or computer software in this article is to specify the experimental procedure. Such identification does not imply recommendation or endorsement by the National Institute of Standards and Technology.

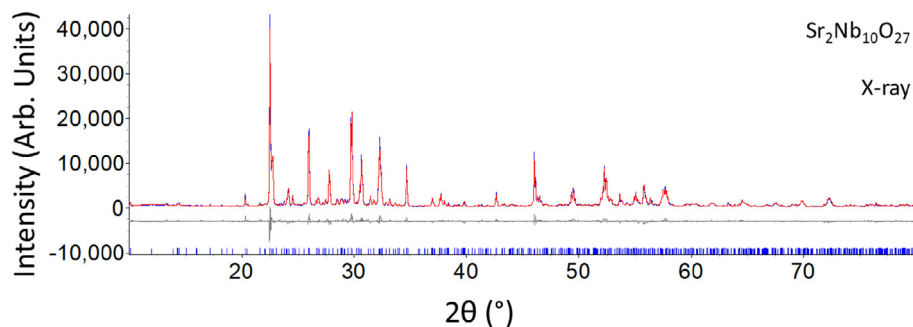


**Fig. 2.** X-ray Rietveld refinement results for  $\text{Sr}_2\text{Nb}_{10}\text{O}_{27}$ . Experimental data is shown in blue, while the calculated pattern is shown in red. The difference between the observed and calculated patterns is shown as a grey line beneath the diffraction patterns. Vertical blue lines at the bottom of the plot represent calculated Bragg positions. (Colour online.)

vided in Table 1 and atomic coordinates for  $\text{Sr}_2\text{Ta}_8\text{O}_{22}$  are provided in Table S2. Fig. S2 shows the results of the X-ray Rietveld refinements. Atomic coordinates for O atoms were not refined since laboratory X-ray data is often of insufficient quality to refine O parameters.

For  $\text{Sr}_2\text{Nb}_{10}\text{O}_{27}$ , a CIF was generated from the neutron refinement and used as a starting point for the X-ray refinement. The O parameters were fixed from the neutron refinement and were not refined against the X-ray data. Refined lattice parameters and atomic coordinates for the X-ray refinement of  $\text{Sr}_2\text{Nb}_{10}\text{O}_{27}$  are shown in Tables 1 and S3, with Fig. 2 showing the results of the X-ray refinement. The X-ray and neutron data were not refined simultaneously due to a long lapse in time between neutron refinements and X-ray data collection/refinement.

### 3. Results and discussion

#### 3.1. Structure

Fig. 3 shows the projection of the TTB structure of  $\text{Sr}_2\text{Nb}_{10}\text{O}_{27}$  along the  $c$ -axis. The TTB structure is built from layers of corner-sharing octahedra stacked along the  $c$ -axis. The Nb atoms are located at layers near  $z \approx 0$ , and all Sr atoms are near  $z \approx \frac{1}{2}$ . The TTB- and TTTB-type compounds can also be viewed as tunnel-containing compounds with the tunnels running as a continuous string of interstitial sites parallel to the  $c$ -axis. In  $\text{Sr}_2\text{Nb}_{10}\text{O}_{27}$ , eight Nb ions adopt a distorted octahedral configuration, while the ninth Nb ion adopts a pentagonal bipyramid configuration. The corner-sharing octahedra form a network that consists of 3-, 4-, and 5-fold

tunnels [9,10]. Both  $\text{Sr}^{2+}$  and  $\text{Nb}^{5+}$  ions are found in the pentagonal tunnels, while only Sr ions were found in the 4-fold tunnels. The size of the 3-fold tunnels is too small to accommodate any alkali cations.

Results of site occupancy refinements indicate that within experimental sensitivity, all Nb sites are fully occupied and all but three of the oxygen sites are fully occupied. The Nb–O bond distances in  $\text{Sr}_2\text{Nb}_{10}\text{O}_{27}$  (with mean distances in the range of 1.946–2.066 Å) are comparable to the Nb–O distances of 1.92(3) Å and 2.11(3) Å found in  $(\text{Ba},\text{Sr})\text{Nb}_2\text{O}_{5.78}$  [12], 1.846(4) Å to 2.160(4) Å in  $\text{SrNb}_2\text{O}_6$  [28], and 1.96 Å to 2.03 Å in  $\text{Nb}_2\text{O}_5$  [29].

The Sr1 and Sr2 ions, both having 12-fold coordination environments (only considering the Sr–O < 3.5 Å distances), occupy the 5-fold tunnels, while Sr3 and Sr4 occupy the 4-fold tunnels. The range of Sr–O distances is large, from 2.41(6) Å to 3.396(26) Å. While Sr vacancies are characteristics of these tunnels, the occupancy of Sr is much higher in the larger 5-fold tunnels.

$\text{Sr}_2\text{Ta}_{10-x}\text{O}_{27-y}$  is isotopic to  $\text{Sr}_2\text{Nb}_{10}\text{O}_{27}$ , but with different site occupancies. In contrast to  $\text{Sr}_2\text{Nb}_{10}\text{O}_{27}$ , where all Nb are fully occupied, there are three Ta deficient sites (Ta2, Ta4, and Ta5) in the  $\text{Sr}_2\text{Ta}_{10-x}\text{O}_{27-y}$  structure. The Ta–O distances (ranging from 1.956 to 2.050 Å) are in agreement with the Ta–O distances found in other compounds: 1.945(4) Å to 2.007(8) Å in  $\text{CaAlTaO}_5$  [30], and 2.00 Å to 2.15 Å in  $\text{Ba}_5\text{Ta}_4\text{O}_{15}$  [31]. The coordination of Sr was found to range from 10- to 12-fold (only considering the Sr–O < 3.5 Å distances), and similar to  $\text{Sr}_2\text{Nb}_{10}\text{O}_{27}$ , the Sr sites are also partially occupied (see Table S2).

The unit cell volume of  $\text{Sr}_2\text{Nb}_{10}\text{O}_{27}$  is unexpectedly slightly greater than that of  $\text{Sr}_2\text{Ta}_{10-x}\text{O}_{27-y}$  (1807.64 Å<sup>3</sup> for  $\text{Sr}_2\text{Nb}_{10}\text{O}_{27}$  vs. 1792.91 Å<sup>3</sup> for  $\text{Sr}_2\text{Ta}_{10-x}\text{O}_{27-y}$ ). The ionic radii of  $\text{Nb}^{5+}$  and  $\text{Ta}^{5+}$

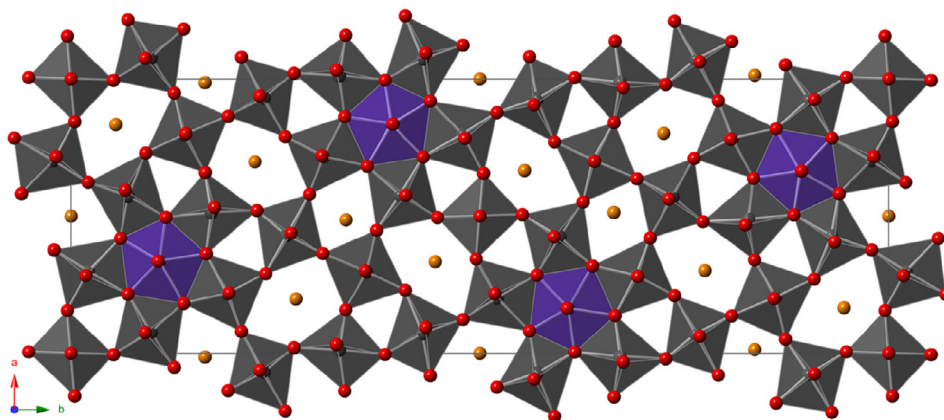


**Fig. 3.** A projection of the structure of  $\text{Sr}_2\text{Nb}_{10}\text{O}_{27}$  along the  $c$ -axis. All distorted octahedral sites are occupied by the Nb ions (grey polyhedra). Infinite 3-, 4-, and 5-fold channels are seen running parallel to the  $c$ -axis. The 4-fold channels are occupied by Sr (orange spheres) and the 5-fold channels are populated by both Sr and Nb. Oxygen is represented as red spheres. (Colour online.)

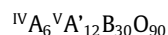
are 0.64 Å for VI-coordination [32]. One possible reason for  $\text{Sr}_2\text{Ta}_{10-x}\text{O}_{27-y}$  to have a smaller unit cell is that there are relatively more vacancies per unit cell in the  $\text{Sr}_2\text{Ta}_{10-x}\text{O}_{27-y}$  compound (discussed below). The effect of the vacancies appears to have a more pronounced effect on the magnitude of the *c*-axis than *a* or *b*, as is evidenced from the significantly shorter *c*-axis of  $\text{Sr}_2\text{Ta}_{10-x}\text{O}_{27-y}$  [3.87903(5) Å] than that of  $\text{Sr}_2\text{Nb}_{10}\text{O}_{27}$  [3.94400(11) Å].

#### 4. Experimental chemical formula for $\text{Sr}_2\text{Nb}_{10}\text{O}_{27}$ and $\text{Sr}_2\text{Ta}_{10-x}\text{O}_{27-y}$

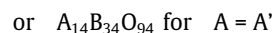
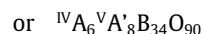
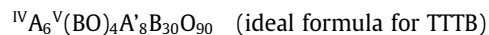
Before analyzing the chemical formula of  $\text{Sr}_2\text{Nb}_{10}\text{O}_{27}$  and  $\text{Sr}_2\text{Ta}_{10-x}\text{O}_{27-y}$  using our experimental results, it will be instructive to first derive the formula for TTB- and TTTB-compounds and their relationships. The chemical formula for a simple TTB compound with the presence of alkaline-earth cations can be written as



where A and A' are alkaline-earth elements occupying the 4- and 5-fold channels, and B is the transition metal. For a TTB compound with a tripled volume, we arrive at the following formula



Next, since the unit cell content of an alkaline-earth free TTTB compound,  $4\text{Nb}_2\text{O}_5$ :  $9\text{WO}_3$  (or  $\text{Nb}_{16}\text{W}_{18}\text{O}_{94}$  with  $Z = 2$ ) [13] can be written as  ${}^{\text{V}}(\text{NbO})_4(\text{Nb}_{12}\text{W}_{18})\text{O}_{90}$ , where four units of NbO are placed in the 5-fold coordination sites, we also place 4 units of (BO) into the 5-fold coordination sites of the  ${}^{\text{IV}}\text{A}_6{}^{\text{V}}\text{A}'_{12}\text{B}_{30}\text{O}_{90}$  formula, giving rise to  ${}^{\text{IV}}\text{A}_6{}^{\text{V}}(\text{BO})_4\text{A}'_8\text{B}_{30}\text{O}_{90}$ . By rearranging this formula, we have derived the ideal TTTB formula to be



The formula  $\text{A}_{14}\text{B}_{34}\text{O}_{94}$  agrees with that derived from our experimental structure if all crystallographic sites are occupied. For a defect strontium tantalate or strontium niobate structure that contains both cation and anion deficient sites, a general chemical formula to describe these compounds could be written as  $\text{Sr}_{14-x}\text{M}_{34-y}\text{O}_{94-z}$  ( $\text{M} = \text{Nb}$  or  $\text{Ta}$ ). The formula for the niobate determined from the neutron Rietveld refinement is:  $\text{Sr}_{8.54(22)}\text{Nb}_{34}\text{O}_{93.52(20)}$ , which is charge-balanced within  $1 - \sigma$ . The formula for the tantalate, determined by Rietveld refinement of X-ray data, is:  $\text{Sr}_{8.68(25)}\text{Ta}_{32.72(46)}\text{O}_{94}$ . This composition does not charge-balance due to excess anionic charge. This can be explained by the fact that we did not refine O occupancies for the tantalate, and so there should be O vacancies to compensate.

A comparison of the unit cell parameters and chemical formula of the alkali-earth containing TTTB- and TTB- compounds reveals that the ratio of the number of transition metal/alkaline-earth element in a formula is important in determining the structure, and hence, the cell parameters. For example, in  $\text{Sr}_2\text{Ta}_{10-x}\text{O}_{27-y}$  and  $\text{Sr}_2\text{Nb}_{10}\text{O}_{27}$ , there is a relatively large ratio of (Nb or Ta) to Sr (4:1 and 5:1) as compares to that in the TTB structure type (i.e. 2:1 in  $\text{SrTa}_2\text{O}_6$ ). As a result, there are more Nb or Ta ions than the available octahedral sites in the simple TTB structure. Some of the Nb and Ta have to go into the pentagonal tunnel sites. The size and shape of the Sr-pentagonal tunnel and the Ta/Nb-pentagonal tunnel are substantially different. Because of the presence of these transition metal tunnels, the repeat distance in the *b*-direction (cell parameter '*b*' of  $\text{Sr}_2\text{Nb}_{10}\text{O}_{27}$  and  $\text{Sr}_2\text{Ta}_{10-x}\text{O}_{27-y}$ ) is tripled as compared with the simple TTB cells (Fig. S1).

#### 4.1. Solid solution formation

From the results of site occupancy calculations, it is clear that the Ta-analogue can form a range of solid solution because of the partial Ta site vacancy. Charge adjustment in this compound is possible by increasing Sr, leading to a solid solution series and smaller Ta/Sr ratio as compared to  $\text{Sr}_2\text{Nb}_{10}\text{O}_{27}$ . The TTB-type solid solution appears to cover a range from  $\text{SrTa}_2\text{O}_6$  to  $\text{SrTa}_4\text{O}_{11}$  (Fig. 2) [14]. A narrow solid solution range in  $\text{Sr}_2\text{Nb}_{10}\text{O}_{27}$  has been identified. It was found that after three heat treatments, the SrO:Nb<sub>2</sub>O<sub>5</sub> of 30:70 composition showed the presence of  $\text{SrNb}_2\text{O}_6$  and  $\text{Sr}_2\text{Nb}_{10}\text{O}_{27}$ . While composition (27:73) is a single phase of the structure type  $\text{Sr}_2\text{Nb}_{10}\text{O}_{27}$ , composition (25:75) showed the presence of Nb<sub>2</sub>O<sub>5</sub> (the characteristic peak of Nb<sub>2</sub>O<sub>5</sub> was located near 47.54° (reflection 0 2 0)) [29], indicating a two-phase region. Furthermore, since there is no solid solution on the Nb-poor side of  $\text{Sr}_2\text{Nb}_{10}\text{O}_{27}$ , there is probably no vacant Nb-site in the structure. The slight 'excess' Nb in the Nb-rich solid solution member is presumably due to an increase of the Sr vacancy, giving rise to a chemical formula of  $\text{Sr}_{2-x}\text{Nb}_{10}\text{O}_{27-z}$  ( $0 \leq x \leq 0.04$ ).

#### 4.2. Bond valence sum calculations of $\text{Sr}_2\text{Ta}_{10-x}\text{O}_{27-y}$ and $\text{Sr}_2\text{Nb}_{10}\text{O}_{27}$

The bond valence sum values, V, for Sr, Ta and Nb were calculated using equations derived by Brown and Altermatt [33]. Values of the reference distance  $r_0$  [Nb–O (1.911 Å), Sr–O (2.118 Å) and Ta–O (1.920 Å)] are tabulated for various pairs of atoms [34]. The bond valence sum of the Sr, Ta, and Nb sites were calculated from the observed distances and the site occupancy obtained from the refinement of neutron data.

The bond valence sum values for  $\text{Sr}_2\text{Ta}_{10-x}\text{O}_{27-y}$  and  $\text{Sr}_2\text{Nb}_{10}\text{O}_{27}$  should only be treated as an approximation because of the complex nature of the defect structures due to the partial occupancy of the oxygen and the metal sites. As an approximation, we can interpret these values only in a qualitative manner in that they reflect the trend of residual strain at a particular site. In  $\text{Sr}_2\text{Ta}_{10-x}\text{O}_{27-y}$  and  $\text{Sr}_2\text{Nb}_{10}\text{O}_{27}$ , V for most Nb and Ta ions are close to the expected value of 5.0. However, the bond valence sums for Sr1 and Sr2 (5-fold tunnels) are significantly less than 2 (1.59 and 1.43 for  $\text{Sr}_2\text{Nb}_{10}\text{O}_{27}$ , and 1.68 and 1.47 for  $\text{Sr}_2\text{Ta}_{10-x}\text{O}_{27-y}$  respectively), indicating an underbonding situation, where the cages that these ions occupy are too large. This result suggests the presence of residual tensile strain at these Sr sites that is not released by distortion. On the other hand, there is compressive residual strain in the Sr3 and Sr4 sites (smaller 4-fold tunnels), which is reflected in the large value of V for Sr4 (2.58) in  $\text{Sr}_2\text{Nb}_{10}\text{O}_{27}$ , for Sr3 (2.87) and for Sr4 (2.72) in  $\text{Sr}_2\text{Ta}_{10-x}\text{O}_{27-y}$ . The neighboring Ta7 octahedra in  $\text{Sr}_2\text{Ta}_{10-x}\text{O}_{27-y}$  and Nb8 octahedra in  $\text{Sr}_2\text{Nb}_{10}\text{O}_{27}$  are also under high compressive strain (bonds too short or overbonded), which was indicated by the high bond valence sum of 5.7 and 5.6 for Nb8 and Ta7, respectively. Table 2 gives

**Table 2**  
Selected bond valence sum values.

Atomic site	BVS	Ideal	Position
<i>Sr<sub>2</sub>Nb<sub>10</sub>O<sub>27</sub></i>			
Nb8	5.7	5	Framework
Sr1	1.59	2	5-fold tunnel
Sr2	1.43	2	5-fold tunnel
Sr4	2.58	2	4-fold tunnel
<i>Sr<sub>2</sub>Ta<sub>10-x</sub>O<sub>27-y</sub></i>			
Ta7	5.6	5	Framework
Sr1	1.68	2	5-fold tunnel
Sr2	1.47	2	5-fold tunnel
Sr3	2.87	2	4-fold tunnel
Sr4	2.72	2	4-fold tunnel

bond valence sum values for the ions where the BVS deviate from expected values.

## 5. Summary

$\text{Sr}_2\text{Ta}_{10-x}\text{O}_{27-y}$  and  $\text{Sr}_2\text{Nb}_{10}\text{O}_{27}$  were determined to be isostructural. Both compounds can be described by the general formula  $\text{Sr}_{14-x}\text{M}_{34-y}\text{O}_{94-z}$  ( $\text{M} = \text{Nb}$  or  $\text{Ta}$ ). While all Nb-sites were found to be fully occupied in  $\text{Sr}_2\text{Nb}_{10}\text{O}_{27}$ , cation vacancies were found for three Ta-sites in  $\text{Sr}_2\text{Ta}_{10-x}\text{O}_{27-y}$ . Charge adjustment in  $\text{Sr}_2\text{Ta}_{10-x}\text{O}_{27-y}$  is possible by increasing Sr content, leading to a solid solution series and smaller Ta/Sr ratio as compared to the Nb/Sr ratio in  $\text{Sr}_2\text{Nb}_{10}\text{O}_{27}$ . Strontium and oxygen vacancies were found in both compounds. Only a small range of solid solution was found in the Nb-compound,  $\text{Sr}_{2-x}\text{Nb}_{10}\text{O}_{27-z}$  ( $0 \leq x \leq 0.04$ ). In the  $\text{SrO-Ta}_2\text{O}_5$  system there appears to be a TTB-type solid solution covering a range from  $\text{SrTa}_2\text{O}_6$  to  $\text{SrTa}_4\text{O}_{11}$ .

## Acknowledgement

Dr. A. Santoro is acknowledged for valuable discussions. We acknowledge the NSF for partial supporting this work through grant DMR-1700030.

## Appendix A. Supplementary data

CCDC 1891738 and 1891739 contains the supplementary crystallographic data for  $\text{Sr}_2\text{Nb}_{10}\text{O}_{27}$  and  $\text{Sr}_2\text{M}_{10-x}\text{O}_{27-y}$ . These data can be obtained free of charge via <http://www.ccdc.cam.ac.uk/conts/retrieving.html>, or from the Cambridge Crystallographic Data Centre, 12 Union Road, Cambridge CB2 1EZ, UK; fax: (+44) 1223-336-033; or e-mail: [deposit@ccdc.cam.ac.uk](mailto:deposit@ccdc.cam.ac.uk). Supplementary data to this article can be found online at <https://doi.org/10.1016/j.poly.2019.06.003>.

## References

- [1] M.H. Francombe, B. Lewis, Structural, dielectric and optical properties of ferroelectric lead metaniobate, *Acta Crystallogr.* 11 (1958) 696.
- [2] N.C. Stephenson, The crystal structure of the tetragonal bronze,  $\text{Ba}_6\text{Ti}_2\text{Nb}_8\text{O}_{30}$ , *Acta Crystallogr.* 18 (1965) 496.
- [3] P.G. Dickens, M.S. Whittingham, The tungsten bronzes and related compounds, *Q. Rev. Chem. Soc.* 22 (1968) 30.
- [4] R.R. Neurgaonkar, W.K. Cory, J.R. Oliver, M. Khoshnevisan, E.J. Sharp, Ferroelectric tungsten bronze crystals and their photorefractive applications, *Ferroelectrics* 102 (1990) 3.
- [5] A. Rotaru, F.D. Morrison, Structural, electrical and relaxor properties of Sc-In solid solution in tetragonal tungsten bronze ceramics, *Ceram. Int.* 45 (2019) 2710.
- [6] Y. Han, M. Yang, Y. Zhang, J. Xie, D. Yin, C. Li, Tetragonal tungsten bronze framework as potential anode for Na-Ion batteries, *Chem. Mater.* 28 (2016) 3139.
- [7] B.N. Parida, P.R. Das, R. Padhee, R.N.P. Choudhary, Ferroelectric, pyroelectric and electrical properties of new tungsten-bronze tantalate, *Curr. Appl. Phys.* 13 (2013) 1880.
- [8] C.P. Heinrich, M. Schrade, G. Cerretti, I. Lieberwirth, P. Leidich, A. Schmitz, H. Fjeld, E. Mueller, T.G. Finstad, T. Norby, W. Tremel, Tetragonal tungsten bronzes  $\text{Nb}_{8-x}\text{W}_{9+x}\text{O}_{47-6}$ : optimization strategies and transport properties of a new n-type thermoelectric oxide, *Mater. Horiz.* 2 (2015) 519.
- [9] E. Bayer, Z. Gruehn, *Anorg. Allg. Chem.* (1963) 149.
- [10] G.W.J.C. Heunen, D.J.W. Ijdo, R.B. Helmholtz,  $\text{SrTa}_4\text{O}_{11}$ : a Rietveld refinement using neutron powder diffraction data, *Acta Crystallogr., Sect. C* 51 (1995) 1723.
- [11] D.C. Craig, N.C. Stephenson, The crystal structure of  $\text{Nb}_8\text{W}_9\text{O}_{47}$ , *Acta Crystallogr., Sect. B* 25 (1969) 2071.
- [12] P.B. Jamieson, S.C. Abrahams, J.L. Bernstein, Ferroelectric tungsten bronze-type crystal structures. I. Barium strontium niobate  $\text{Ba}_{0.27}\text{Sr}_{0.75}\text{Nb}_2\text{O}_{5.78}$ , *J. Chem. Phys.* 48 (1968) 5048.
- [13] R.S. Roth, J.L. Waring, Phase equilibria related to crystal structure in the system niobium pentoxide-tungsten trioxide, *J. Res. Natl. Bur. Stand., Sect. A* (1966) 281.
- [14] W. Wong-Ng, R.S. Roth, B.H. Toby, J.Y. Cahn, J. Dillingham, T.A. Vanderah, The Binary System  $\text{SrO-Ta}_2\text{O}_5$ , Phase Diagrams for Electronic Ceramics 1, EC-131, The American Ceramic Society, Westerville, Ohio, 2003, p. 82.
- [15] P.P. Leshchenko, A.V. Shevchenko, L.N. Lykova, L.M. Kovba, E.A. Ippolitova, The system  $\text{SrO-Nb}_2\text{O}_5$ , *Inorg. Mater.* 1013 (1982).
- [16] P. Leshchenko, V.P. Kobzareva, L.N. Lykova, L.M. Kovba, *Russ. J. Inorg. Chem.* (1980) 1011.
- [17] P.P. Leshchenko, A.V. Shevchenko, L.N. Lykova, L.M. Kovba, E.A. Ippolitova, Strontium oxide-niobium(V) oxide system, *Izv. Akad. Nauk SSSR Neorg. Mater.* 18 (1982) 1202.
- [18] M.J. Dejneka, C.L. Chapman, S.T. Misture, Strong, low thermal expansion niobate ceramics, *J. Am. Ceram. Soc.* 94 (2011) 2249.
- [19] J. Leitner, I. Sipula, K. Ruzicka, D. Sedmidubsky, P. Svoboda, Heat capacity, enthalpy and entropy of strontium niobates  $\text{Sr}_2\text{Nb}_{10}\text{O}_{27}$  and  $\text{Sr}_3\text{Nb}_4\text{O}_{15}$ , *J. Alloys Compd.* 481 (2009) 35.
- [20] X. Gasperin, *Bull. Soc. Fr. Mineral. Crystallogr.* (1963) 386.
- [21] J. Baker-Jarvis, B.F. Riddle, *Natl. Inst. Stand. Technol. Tech. Note* (1996) 1384.
- [22] H.M. Rietveld, Profile refinement method for nuclear and magnetic structures, *J. Appl. Crystallogr.* 65–71 (1969).
- [23] R.A. Young, Editor the Rietveld Method, *Int. Union Crystallogr. Monogr. Crystallogr., Oxford Univ. Press*, 1993.
- [24] L.B. McCusker, R.B. Von Dreele, D.E. Cox, D. Louer, P. Scardi, Rietveld refinement guidelines, *J. Appl. Crystallogr.* (1999) 36.
- [25] A.C. Larson, R.B.V. Dreele, General Structure Analysis System (GSAS), Los Alamos National Laboratory Report, 2000, pp. 86–748.
- [26] B.H. Toby, EXPGUI, a graphical user interface for GSAS, *J. Appl. Crystallogr.* 34 (2001) 210.
- [27] A. Coelho, TOPAS and TOPAS-academic: an optimization program integrating computer algebra and crystallographic objects written in C++, *J. Appl. Crystallogr.* 51 (2018) 210.
- [28] V.K. Trunov, I.M. Averina, Y.A. Velikodnyi, Refining the crystal structure of strontium niobate ( $\text{SrNb}_2\text{O}_6$ ), *Kristallografiya* (1981) 390.
- [29] B.M. Gatehouse, A.D. Wadsley, The crystal structure of the high temperature form of niobium pentoxide, *Acta Crystallogr.* 17 (1964) 1545.
- [30] M. Sales, G. Eguia, P. Quintana, L.M. Torres-Martinez, A.R. West, The phase diagram  $\text{CaO-Al}_2\text{O}_3\text{-Ta}_2\text{O}_5$  and the crystal structures of  $\text{Ca}_2\text{AlTaO}_6$  and  $\text{CaAlTaO}_5$ , *J. Solid State Chem.* 143 (1999) 62.
- [31] F. Galasso, L. Katz, Preparation and structure of  $\text{Ba}_5\text{Ta}_4\text{O}_{15}$  and related compounds, *Acta Crystallogr.* 14 (1961) 647.
- [32] R.D. Shannon, Revised effective ionic radii and systematic studies of interatomic distances in halides and chalcogenides, *Acta Crystallogr., Sect. A* 32 (1976) 751.
- [33] I.D. Brown, D. Altermatt, Bond-valence parameters obtained from a systematic analysis of the inorganic crystal structure database, *Acta Crystallogr., Sect. B* 41 (1985) 244.
- [34] N.E. Brese, M. O'Keeffe, Bond-valence parameters for solids, *Acta Crystallogr., Sect. B* 47 (1991) 192.